Title: Tunable Zero-Field Magnetoresistance Responses in Si Transistors: Origins and Applications

Authors: Stephen J. Moxim[1,a], Nicholas J. Harmon[2], Kenneth J. Myers[3*], James P. Ashton[3**], Elias B. Frantz[3***], Michael E. Flatte[4], Patrick M. Lenahan[3], Jason T. Ryan[1]

[1]Alternative Computing Group, National Institute of Standards and Technology, Gaithersburg, Maryland 20899, USA

[2]Department of Physics and Engineering Science, Coastal Carolina University, 100 Chanticleer Dr E, Conway, South Carolina 29528, USA

[3]Department of Engineering Science and Mechanics, The Pennsylvania State University, 201 Old Main, University Park, Pennsylvania 16802, USA

[4]Department of Astronomy and Physics, University of Iowa, 101 Jessup Hall, Iowa City, Iowa 52242, USA

[*]Current Address: Northrop Grumman, 1212 Winterson Rd, MS 3010, Linthicum Heights, Maryland 21090, USA

[**]Current Address: Keysight Technologies Inc., Santa Rosa, California 95403, USA

[***]Current Address: Intel Corporation, 2501 NE Century Blvd, Hillsboro, Oregon 97124, USA

[a]corresponding author email: stephen.moxim@nist.gov

Abstract: The near-zero-field magnetoresistance (NZFMR) response has proven to be a useful tool for studying atomic-scale, paramagnetic defects that are relevant to the reliability of semiconductor devices. The measurement is simple to make and, in some cases, simple to interpret. In other cases, more sophisticated modeling based on the stochastic Liouville equation (SLE) is needed to access valuable information from NZFMR results. It has been shown that hyperfine and dipolar coupling interactions at atomic-scale defects affect the NZFMR lineshape, but experimental parameters related to the detection method of NZFMR can also affect the

nature of the response. Here, we demonstrate four distinct NZFMR detection methods in Si

MOSFETs which all access identical Si/SiO$_2$ interface defects. In all four cases, we show that the

lineshape of the response is tunable based on experimental parameters alone. Using SLE-based

modeling, we verify that time constants connected to physical carrier capture rates at the defect

sites lead to these NZFMR lineshape changes. The results demonstrate a method to extract some

atomic-scale information for the purpose of defect identification. They also have broader

applications to the continued development of ultra-sensitive magnetometers based on NZFMR in

semiconductors. Additionally, the NZFMR effect in common Si-based devices may provide an

inexpensive and accessible platform that mimics similar radical pair mechanisms that have

become increasingly important in various biology fields.

I.   Introduction

The near-zero-field magnetoresistance (NZFMR) effect arises from the presence of

paramagnetic defects in the electrically active regions of semiconductor devices. In recent years,

the effect has been explored as an experimentally simpler alternative to electrically detected

magnetic resonance (EDMR) measurements for studying the chemical and physical nature of

atomic-scale traps in semiconductors and insulators.[1–9] Recent experimental work on the Si/SiO$_2$

system has shown that NZFMR can provide information about electron-nuclear hyperfine

interactions at some trapping centers through relatively straightforward analysis.[5,6] In some

cases, this is sufficient information to infer the chemical and physical identity of the traps.

More extensive analysis of NZFMR responses has revealed additional information about

electron-nuclear hyperfine interactions at defect sites in the Si/SiO$_2$ system. This was

accomplished via theoretical models developed from the stochastic Liouville equation (SLE).[3,4,7] They are analogous to models developed in the field of organic magnetoresistance (OMAR),[10–17] an effect observed in organic semiconductor materials which is similar in origin to NZFMR. Such models generally attribute the shape of the response to two factors: 1) the hyperfine coupling with nearby magnetic nuclei (and/or dipolar coupling with other unpaired electrons), and 2) a set of kinetic rate constants that describe the spin-dependent transport through the defect centers.

Tunability of the NZFMR lineshape, independent of any change in hyperfine or dipolar interactions, has been observed previously using several different detection schemes[8,18]. Such results can make the interpretation of results in terms of defect properties difficult. An understanding of how detection method parameters affect the nature of the NZFMR response is desirable for those concerned with the atomic-scale nature of trapping centers in semiconductor devices. A more complete understanding of the origin of the NZFMR lineshape is also important to those working on the development of deep-space magnetometers based on the response. The sensitivity of these sensors is determined by both the size and shape of the NZFMR response, and optimizing the response is key to further improvements.[19] Finally, the physical origins of NZFMR are common to several phenomena observed in the field of quantum biology,[20,21] and can be modeled in a similar way. NZFMR in widely available and inexpensive Si-based semiconductor devices may produce results relevant to the study of these phenomena.

A. Near-Zero-Field Magnetoresistance Detection

NZFMR can be detected in any semiconductor device current that involves electron capture at defect centers which already contain an unpaired electron spin (the same defects that would be considered EDMR-active). NZFMR has been detected via spin-dependent recombination (SDR) in diodes and metal-oxide-semiconductor field effect transistors (MOSFETs),[1,5,8,9,22] and via spin-dependent tunneling currents in capacitors and MOSFETs.[2,6,23–25] This work will focus only on NZFMR detected via SDR. A decades-long body of literature concerning SDR and EDMR measurements exists, beginning with SDR photocurrents in bulk silicon measured by Lepine in 1972.[26] Subsequent work has improved upon Lepine's initial model,[27–29] and it has recently been adapted to better describe NZFMR.[3] SDR can be understood at a practical level by considering Shockley-Read-Hall (SRH) recombination[30] with the addition of basic spin physics, as illustrated in Figure 1.
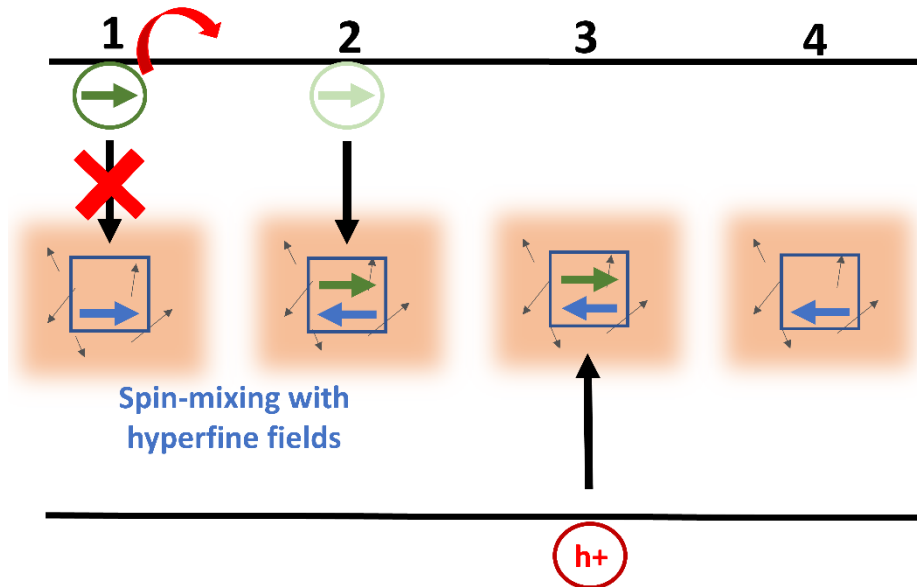

Fig. 1. Conceptual illustration of SDR NZFMR. 1) To begin the process, a conduction band electron drops into a shallow state and forms a spin pair with a defect electron. If the spin pair is a triplet, the first electron eventually dissociates back to the conduction band. 2) Spin-mixing with local magnetic fields at the defect site facilitates the conversion of some triplet

pairs to singlets, allowing the first electron to drop into the defect. 3) After some time, a hole

is captured at the same defect and recombination occurs. 4) The defect is left empty and the

process can start again.

The SRH recombination process requires defects with energy levels near the middle of the

bandgap and a supply of both electrons in the conduction band and holes in the valence band. In

the simplest picture, an electron is first captured at a defect center. Sometime later, a hole is

captured at the same defect center (in other words, the captured electron drops to an empty spot

in the valence band). If the defect center already contains an unpaired electron spin (it starts the

process in a paramagnetic state), the Pauli exclusion principle becomes important to the electron

capture step of SRH recombination. Here, the electrons form an intermediate spin pair,[3,29] and

recombination is only allowed in the case of a singlet pair. The application of an external

magnetic field can alter the relative populations of singlet and triplet pairs, which in turn makes

the probability of recombination dependent on the strength of the applied field. While electron

capture (steps 1 and 2 in Fig. 1) is usually invoked to explain the NZFMR response, it is possible

that hole capture (step 3 in Fig. 1) could also contribute. The NZFMR response is obtained by

measuring the recombination current while the applied field is swept across zero. In most cases,

the change in current consists of at least two features: a relatively broad peak, and a more narrow

feature which can be described as having the opposite magnetoresistance. The response is always

symmetric about zero applied field, and the sign of the respective features depends on the

detection method. The exact nature of the field-dependent recombination (the amplitude and

width of each feature) depends on the local magnetic environment of the defects, which is

typically dominated by electron-nuclear hyperfine interactions. Strong hyperfine interactions can

cause the appearance of additional features, farther away from zero applied field, which can be used to identify defects with previously known hyperfine coupling constants[5]. These details all contribute to the final NZFMR lineshape observed experimentally.

To observe the SDR effect in general, both electrons and holes must be accessible to traps which are able to capture both types of charge carriers. In this work, we are most concerned with Si/SiO_2 interface traps in MOSFETs and capacitors. For the case of MOSFETs, the simplest SDR technique is the dc I-V biasing scheme (also called the gated diode measurement, or sometimes simply "SDR").[31] In this measurement, the source and drain are shorted together and forward biased below the built-in diode voltage. This injects some minority carriers toward the interface region. A gate bias is selected such that roughly equal populations of minority carriers from the diode contacts and majority carriers from the bulk substrate are present near the interface traps. The recombination current (and thus SDR current) is measured through the substrate contact; it is due to the diffusion of majority carriers toward the interface to replace those annihilated by recombination events. dc I-V measurements are limited in sensitivity when using a high diode voltage (V_F) since the recombination current is detected through the body contact. At high values of V_F, the body current due to recombination is overwhelmed by source-to-body and drain-to-body current. The dc I-V biasing scheme is illustrated in Figure 2a.

A similar technique, known as the bipolar amplification effect (BAE) measurement,[32] circumvents this sensitivity issue by detecting the SDR response from interface traps through the drain contact, rather than the body. In BAE, the source is forward biased to inject minority carriers towards the interface. The body is grounded, and the gate voltage is selected such that an equal number of majority and minority carriers are present at the interface. The current change due to recombination is measured at the drain; it is observed as a reduction in current due to

minority carriers which are annihilated by the recombination process before traversing the entire channel. The roles of the source and drain contact can be reversed if desired. The BAE biasing scheme is illustrated in Figure 2b. Both dc I-V and BAE have the advantage of being very simple and inexpensive dc measurements.

Charge pumping (CP)[33] can also be used to generate SDR current from recombination at MOSFET interface traps. The CP setup is shown in Figure 2c. The source and drain are grounded, and an arbitrary waveform generator applies a trapezoidal voltage waveform to the gate at the charge pumping frequency (F_{CP}). The trapezoidal waveform is set up such that V_{Low} and V_{High} lie outside of the flatband voltage, V_{fb}, and the threshold voltage, V_{th}. When this is the case, V_{High} floods the MOSFET interface with minority carriers, which become trapped at defect sites. In an n-channel MOSFET, these carriers are electrons which diffuse in from the grounded source and drain. When the voltage is switched to V_{Low}, the interface floods with majority carriers (holes in the case of an n-channel MOSFET), and recombination events occur at the interface defects at a rate of once per defect, per cycle. The recombination current is measured at the substrate contact as majority carriers diffuse in to replace those annihilated by recombination.

All the above techniques require source and drain contacts to act as sources of one type of carrier. This seemingly makes SDR impossible to observe in simple Si/SiO_2 capacitor structures. While technically true, another ac technique is able to circumvent this problem and produces an SDR-like effect in capacitors without the need for source and drain contacts. This technique is known as spin-dependent transient spectroscopy (SDTS). The first SDTS EDMR measurements were made by Chen and Lang in 1983. The technique was then referred to as spin-dependent thermal emission.[34] Recently the technique has been revived and refined by Myers et al.[35] To conduct the measurement on a $p-Si/SiO_2$ capacitor, the top gate is first held at a sufficient

positive voltage such that electrons fill the interface traps. A short pulse is then applied to a

negative voltage to empty the traps of their electrons. When the voltage returns to its positive

value, the traps are refilled with electrons. The resulting transient can be measured through the

substrate and fed into a boxcar integrator. The boxcar gates the current measurement to only the

electron-capture transient, just after the pulse is released (the exact timing and size of the

measurement window are adjustable). The biasing conditions for SDTS are illustrated in Figure

2d. While not identical to traditional SDR, SDTS shares the same spin-dependent step as the

SDR methods above. It has other advantages as well; it is a room temperature measurement that

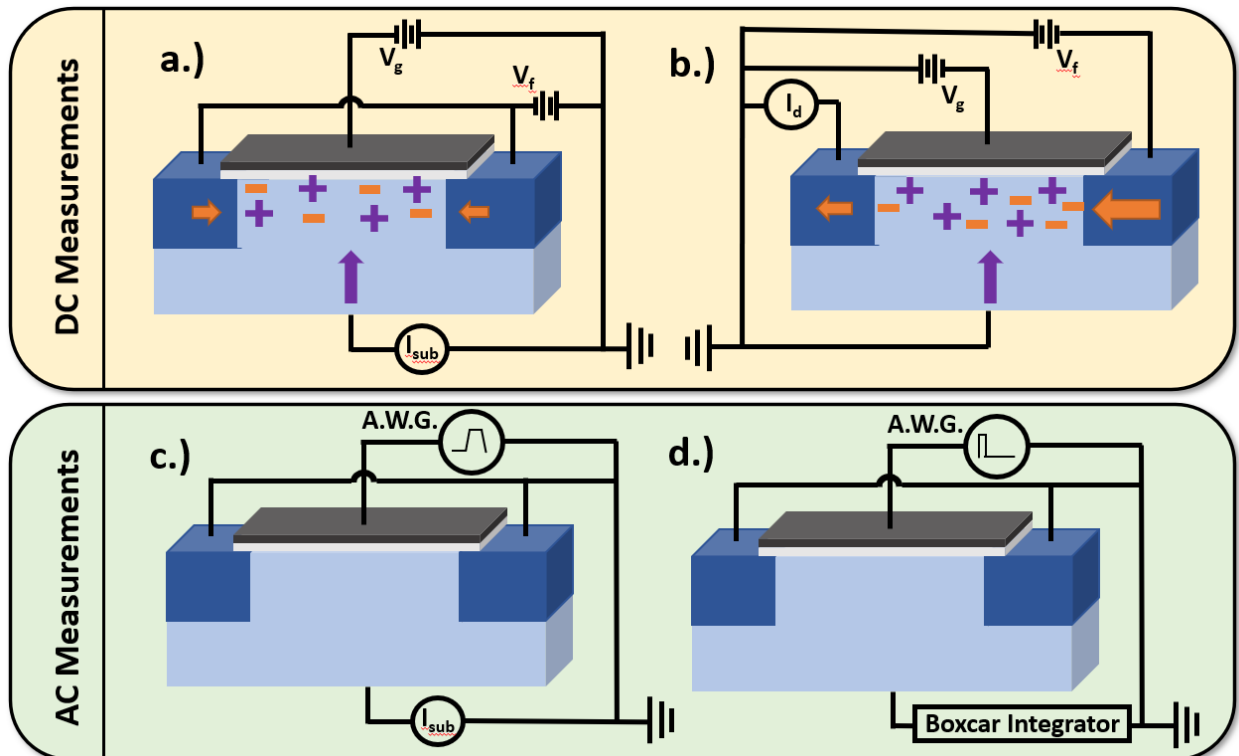can provide some energy level resolution of interface defects.[35]

Fig. 2. DC and AC EDMR/NZFMR biasing conditions for MOSFETs: a) dc I-V, b) BAE, c)

charge pumping, and d) SDTS.

B. Si/SiO$_2$ Interface Traps

It is impossible to overstate the relevance of Si-based semiconductor devices, and the Si/SiO$_2$ system has easily been the most studied using NZFMR. This work will focus on the NZFMR response due to traps (defects) at the Si/SiO$_2$ interface.

These defects are well understood but continue to be relevant to device processing and MOSFET reliability issues decades after their initial characterization. In the case of (111)Si/SiO$_2$ interfaces, only a single defect center exists: the P$_b$ center[36]. It is described as a dangling bond residing on a Si atom which itself is back-bonded to three other Si atoms. The dangling bond is pointed into the SiO$_2$ layer normal to the interface, and it contains one unpaired electron when neutrally charged.

We utilize only devices with (100)Si/SiO$_2$ interfaces, for which the defect chemistry is more complex. In this case, the dominant defect is known as the P$_{b0}$ center[37]. It is chemically and physically identical to the (111) P$_b$ center, and also points into the SiO$_2$ layer along the (111) family of directions. This makes multiple orientations of the P$_{b0}$ center possible at the (100) interface. In its paramagnetic, neutral charge state, it contains one unpaired electron. By losing an electron, it is converted to a spin-0, positively charged state. By capturing a second electron, it is converted to a diamagnetic, negatively charged state. The P$_{b0}$ center has a broad energy level distribution, centered in the middle of the Si bandgap. Defects capturing their first electron are lower in energy than those capturing their second electron. Thus, the distribution is composed of two overlapping peaks, where the lower energy peak corresponds to the transition between positive and neutral charge states (the capture of the first electron) and the higher energy peak

corresponds to the transition between the neutral and negative charge states (the capture of the second electron). Conley and Lenahan,[38] and references therein, provide a detailed review of the P_b and P_{b0} interface defects from an electron spin resonance perspective. A second defect, the P_{b1} center,[39] can also be present at the (100) interface, but it exists in smaller quantities.[40,41] The P_{b1} defect is similar to the P_{b0} but differs in the symmetry of the three back-bonded Si atoms. It has a narrower energy level distribution than the P_{b0} but is also centered near the middle of the Si bandgap. Combinations of P_{b0} and P_{b1} defects have been studied via NZMFR in the past, and several hyperfine values for the defect centers have been extracted.[4,5] Typically, all Si/SiO_2 interface defects experience hyperfine interactions from ^{29}Si atoms and nearby ^1H atoms.

Its important to note that oxide dangling bond defects also exist in the Si/SiO_2 system, and are known as E' centers. For the purposes of this work, they are not considered due to previous EDMR results from the same/similar device structures which indicate that interface traps dominate the SDR response[35,40].

II.   Experiment Details

The NZFMR results presented here are taken on two types of Si/SiO_2 structures. The dc I-V, BAE, and CP NZFMR results were made on arrays of 126 n-channel Si MOSFETs with 7.5 nm thick SiO_2 gate dielectrics. The MOSFETs were wired in parallel to allow equivalent biases to be applied to all 126 devices simultaneously. High-field gate stressing was used to create a high interface defect density on the order of 1×10^{12} defects/cm^2, described in previous work[40]. The SDTS NZFMR measurements were made on large area (8×10^{-3} cm^2) Si/SiO_2 capacitors with 50 nm thick SiO_2 layers. The NZFMR spectrometer consisted of a nested set of Hemholtz coils capable of sweeping fields up to 20 mT and powered by a bipolar DC power supply. The device

current was monitored and fed to a current-to-voltage preamplifier, and then to a lock-in amplifier. Magnetic field modulation was accomplished by a smaller set of magnetic field coils at frequencies ranging from 210 Hz to 1 kHz. The lock-in amplifier output produces an approximate derivative of the NZFMR current with respect to magnetic field; the results were integrated to show the actual change in device current for clarity. Signal averaging on the scale of several hours was used to further increase the signal-to-noise ratio. In all cases shown here, the NZFMR response consisted of a broad feature and an ultra-low-field feature. The majority of lineshape changes observed occur in the ultra-low-field region, and the plots in this work are cropped to highlight this region.

III.   Results/Modeling

A. AC Measurements

SDTS NZFMR provides the most direct link between electronic capture rates and the kinetic rates associate with NZFMR. The SDTS NZFMR results of Figure 3a and Figure 3b were measured in large area Si/SiO_2 capacitors. V_{high} was set at -1.5 V (strong inversion) and V_{low} was set to -7.5 V (strong accumulation)[35]. The pulse frequency was 14.1 kHz, and the boxcar gate width was set to 500 ns. The measurement delay, which we will refer to as t_{boxcar}, was varied between 0 µs and 9 µs after the switch to V_{high} to probe the SDR kinetics along different portions of the current transient. This current transient (in identical capacitors) has been directly relate to capture at P_{b0} centers in previous work.[35] The results of Figure 3b are normalized to the amplitude of the broad NZFMR feature to highlight the differences in lineshape. It is clear that the NZFMR response narrows, and the ultra-low-field inflection point decreases in amplitude as the measurement window is moved later along the transient. The position of the measurement

window along the current transient (Figure 3a) directly represents the "speed" of electron

trapping events at Si/SiO$_2$ interface defects, with each defect capturing its first electron spin-

independently, followed by a second electron capture which can be spin-dependent. Therefore,

the transient includes both the spin-independent first electron capture, and the spin-dependent

second electron capture. The "speed" of the trapping event is related to the energy level of the

defect relative to the conduction band. The energy level distributions of Si/SiO$_2$ interface defects

are broad, and the distributions for empty and singly-occupied defects overlap significantly.

Because of this, some defects capture the second electron before others capture the first, and thus

a spin-dependent response can be seen even very early in the transient. This was confirmed by
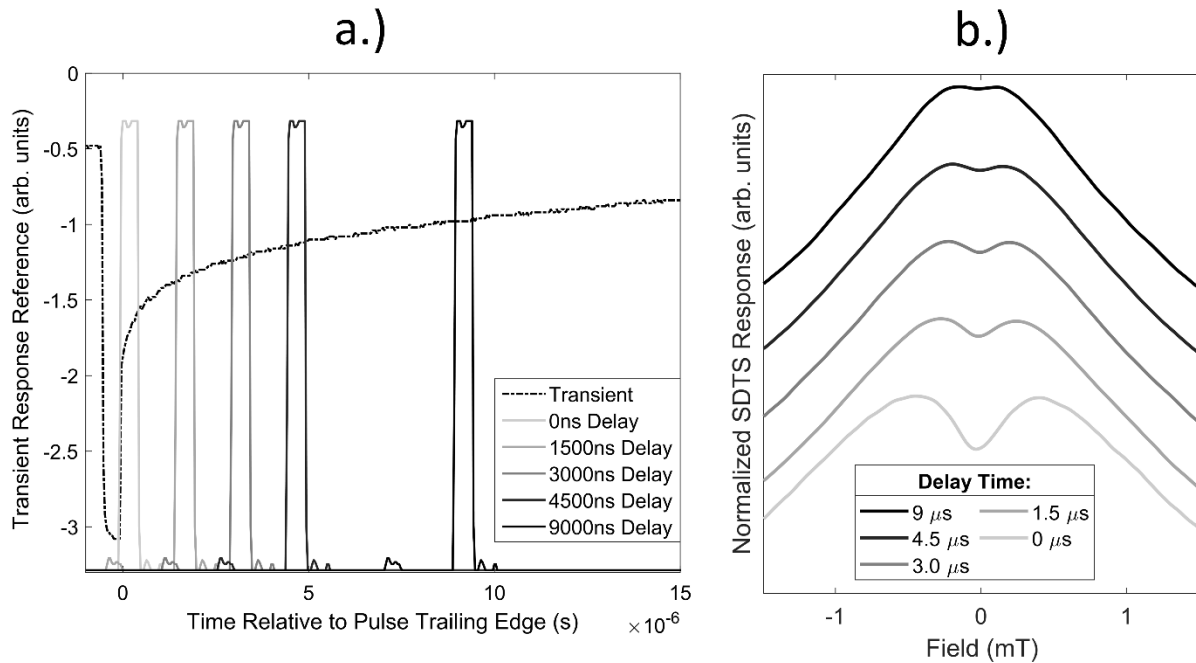
previous EDMR results[35].

Fig. 3. a) Current transient in Si/SiO$_2$ capacitor, and boxcar averaging windows used. b) SDTS NZFMR results at each averaging window used. The NZFMR results are normalized to the amplitude of the broad feature and offset to highlight the differences in lineshape.

Charge pumping NZFMR measurements were also made on Si MOSFETs with 7.5 nm thick SiO$_2$ gates. The charge pumping waveform used is illustrated in Figure 4a. The normalized NZFMR results are shown in Figure 4b for charge pumping frequencies of 1 MHz, 3 MHz, and 5 MHz. An overall broadening of the spectrum and increase in the size of the ultra-low-field inflection relative to the broader portion of the responses are observed as frequency is increased. This trend is reminiscent of (although more drastic than) that observed in the SDTS NZFMR results of Figure 3b. The charge pumping NZFMR results are consistent with those reported by Anders et al.[8] in SiC MOSFETs with SiO$_2$ gate dielectrics. The results of Figure 4 confirm that the trend in NZFMR lineshape with increasing F$_{CP}$ is not material-dependent.
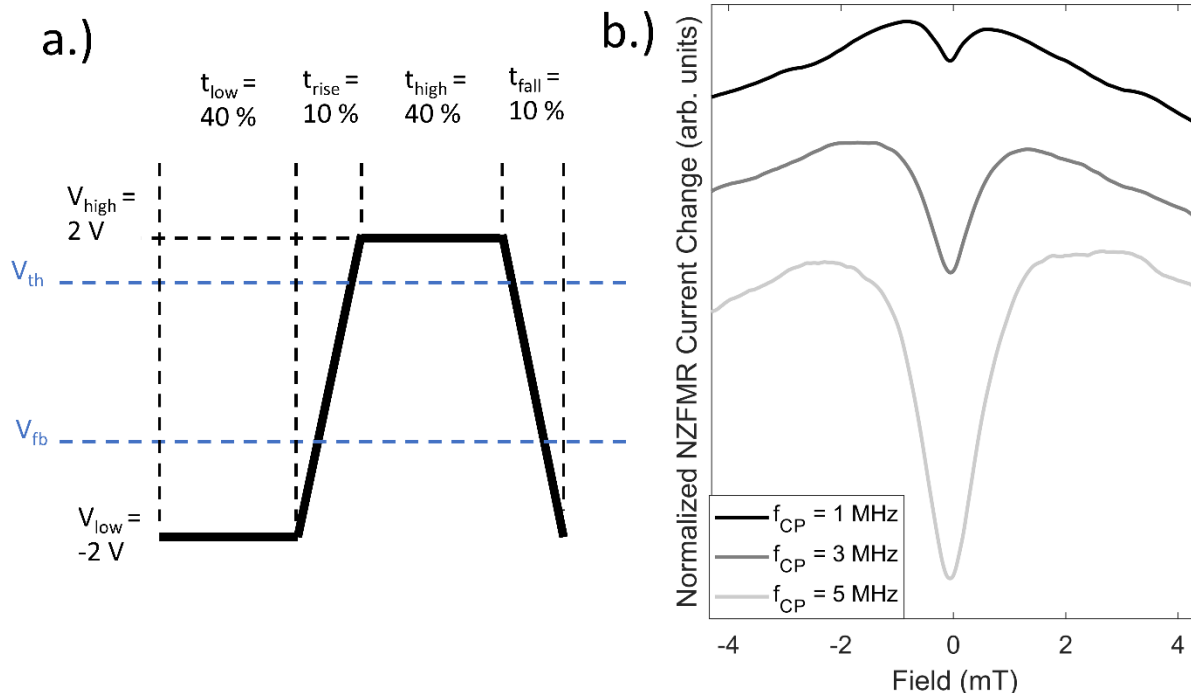
Fig. 4. a) charge pumping waveshape utilized (not to scale), and b) charge pumping NZFMR results for three values of charge pumping frequency. The NZFMR results are normalized to the amplitude of the broad feature and normalized to highlight the differences in lineshape.

B. DC Measurements

The normalized dc I-V and BAE NZFMR results are shown in Figure 5a and 5b, respectively, for a variety of diode forward biases. The same Si/SiO_2 MOSFETs used for the charge pumping NZFMR measurements were used here. The trends of an overall broadening of the response and an increase in the relative amplitude of the ultra-low-field feature are seen again in the DC measurement results, and in this case they correspond to an increase in diode forward bias. The effect is more dramatic in the BAE NZFMR results because higher forward biases can be used while maintaining reasonable sensitivity. Both dc I-V and BAE

offer the same control over the NZFMR lineshape as the AC measurements but are more
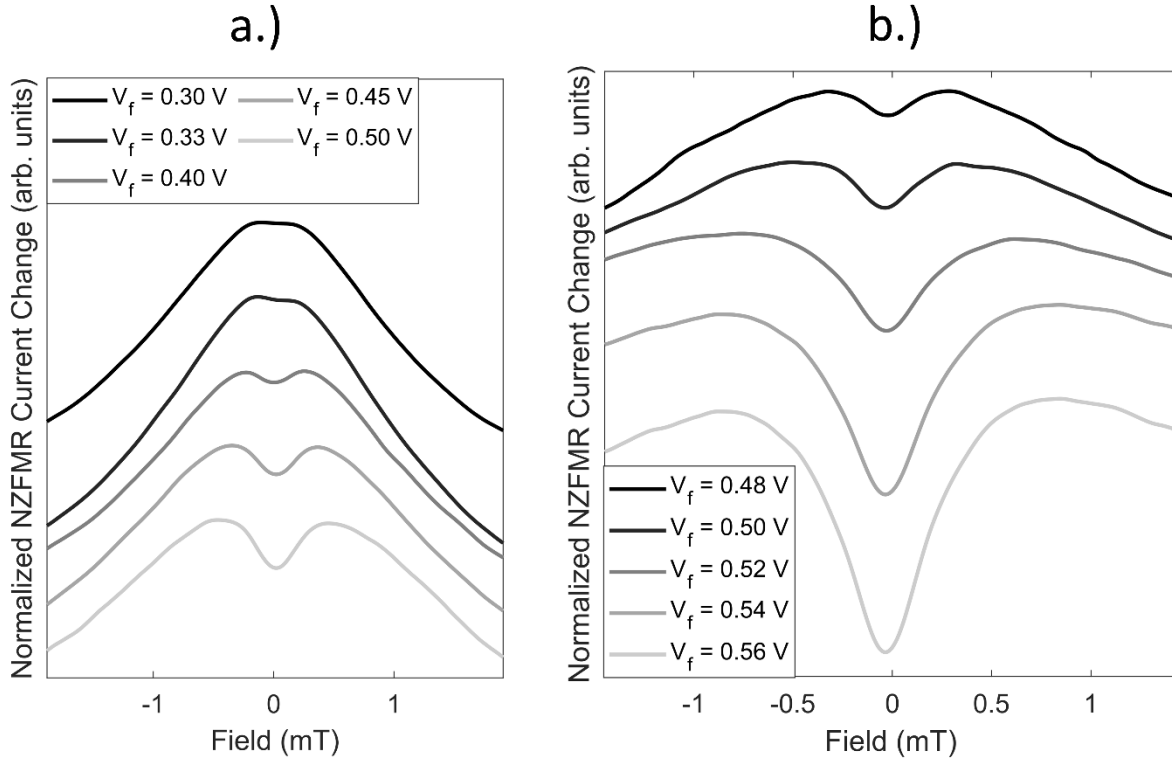
inexpensive and simpler in comparison.

Fig. 5. dc I-V NZFMR results (a) and BAE NZFMR results (b) as a function of diode forward

bias. The NZFMR results are normalized to the amplitude of the broad feature and normalized to

highlight the differences in lineshape.

C. NZFMR Modeling

The processes of coherent spin evolution and stochastic spin-dependent capture and

dissociation at the defect are ideally suited for the stochastic Louiville equation which has been

previously employed for recombination current and trap-assisted transport calculations[3,4]. In this

framework, the key quantity to determine is ρ_s which is the probability of the two electron spins

in Figure 1 (steps 1-2) forming a singlet pair (which allows for electron capture at the defect). Through modeling NZFMR lineshapes, hyperfine couplings and carrier capture times are estimated. We choose to develop this modeling framework around the SDTS NZFMR data because SDTS offers the most direct connection to physical carrier capture time constants.

To determine ρ_s, we solve for the spin-density matrix ρ which fully accounts for not only the spin and charge dynamics at the defect but also the evolution of the spin pair (shown in Figure 1, steps 1-2) undergoing any number of spin interactions with other paramagnetic defects or nuclear spins. This evolution is governed by the stochastic Liouville equation:

$$\frac{\partial \rho}{\partial t} = -i\,\hbar\,[H,\rho] - \frac{k_S + k_D}{2}\{P_S,\rho\} - (k_T - \frac{k_D}{2})\{P_T,\rho\}$$

Here, $\hbar$ is the reduced Planck's constant, and P_S and P_T are singlet and triplet projection operators, respectively. H is the spin Hamiltonian, with $H = g\mu_B B_0 \cdot (S_1 + S_2) + g\mu_B B_{n,1} \cdot S_1 + g\mu_B B_{n,2} \cdot S_2$ where $B_{n,i}$ are classical nuclear magnetic field vectors with each component drawn from a Gaussian distribution of width a_i. This approximation for the nuclear field is sensible since a large number of magnetic nuclei (^{29}Si and H)[3,4] interact with each of the two interfacial electron spins. The initial condition assumes that all electronic spin states are equally likely since the singly-occupied spin and the incoming conduction spin are randomly oriented. The first term on the right-hand side is the Liouville or Neumann equation for the density matrix, describing the coherent evolution of the density matrix. The second and third terms signify the random processes of spin capture and spin dissociation of the spin pairs which in general may depend on their spin configuration (singlet or triplet recombination occurs at rates k_S and k_T, respectively). Assuming small spin-orbit interactions, we take $k_T = 0$; triplets are not captured by the deep defect. The rate of singlet capture depends on the occupation of states so is written as

$k_S Tr[P_S \rho(t)] = k_S \rho_S(t)$. A rate k_D describes the dissociation of the spin pair. The transient current is expected to be proportional to $k_S \rho_S(t)$.

This equation does not attempt to describe the spin-independent capture at the traps. Traps must first be singly occupied (they must spin-independently capture their first electron) before they can be doubly occupied (spin-dependently). For this reason, the values we compute the NZFMR for do not align with the experimental boxcar windows. Extending our density matrix approach to include the stage of spin-independent capture is beyond the scope of this work but is, in principle, possible within our framework. An extension to include the potential spin-dependence of hole capture (step 3 in Fig. 1) is also theoretically possible, but is not appropriate for the case of SDTS where electron capture is isolated.

Additionally, due to the laboratory results necessarily combining spin-dependent and spin-independent capture, the model's amplitudes should not be compared to the experiments since the relative populations of unoccupied, singly occupied, and doubly occupied defects are unknown. Therefore, our focus is solely on the lineshapes produced by the model.

Due to the extensive time needed for hyperfine averaging, non-linear fits to the data are not feasible. Even a systematic manual variation of all parameters a_1, a_2, k_S, k_D is not possible. Instead, we rely on previous results on Si/SiO$_2$ MOSFETs[3] that found suitable hyperfine constants 0.5 mT, 0.15 mT, and $k_D = 0.00125$ ns^{-1}. We then varied k_S which we expect to have a much larger effect on response than the spin-independent rate k_D, since k_S directly relates to the rate of spin-dependent capture.

At different times, different defect energies are involved in the spin-dependent capture, and different populations of carriers are present near the defects. Since the rate of capture depends on

defect depth, we compute $\rho_S(t)$ for a range of k_S over a range of t_{boxcar}. We constrain k_S by

$k_S(t_{n+1}) > k_S(t_n)$ for the nth boxcar. The procedure yields a qualitative correspondence to the

experimental results as shown in Figure 6. In our modeling, we take t_{boxcar} to be the measurement

at a single time and not over a window of times which occurs in the SDTS experiments. Thus,

the capture time is equal to t_{boxcar} whereas experimentally, a small range of capture times occur

over the boxcar window. On the other hand, k_s is a parameter characteristic of the system at a

given time that also depends on the energy difference between defect and the captured electron.

Our modeling shows that the picture of defect filling at various boxcar times is consistent

with the experiment. To provide a more rigorous defense will require the inclusion of spin-

independent capture as well; however, for the purposes of this article, the simpler framework

presented here for SDTS suffices to demonstrate the line shape alterations arising from accessing

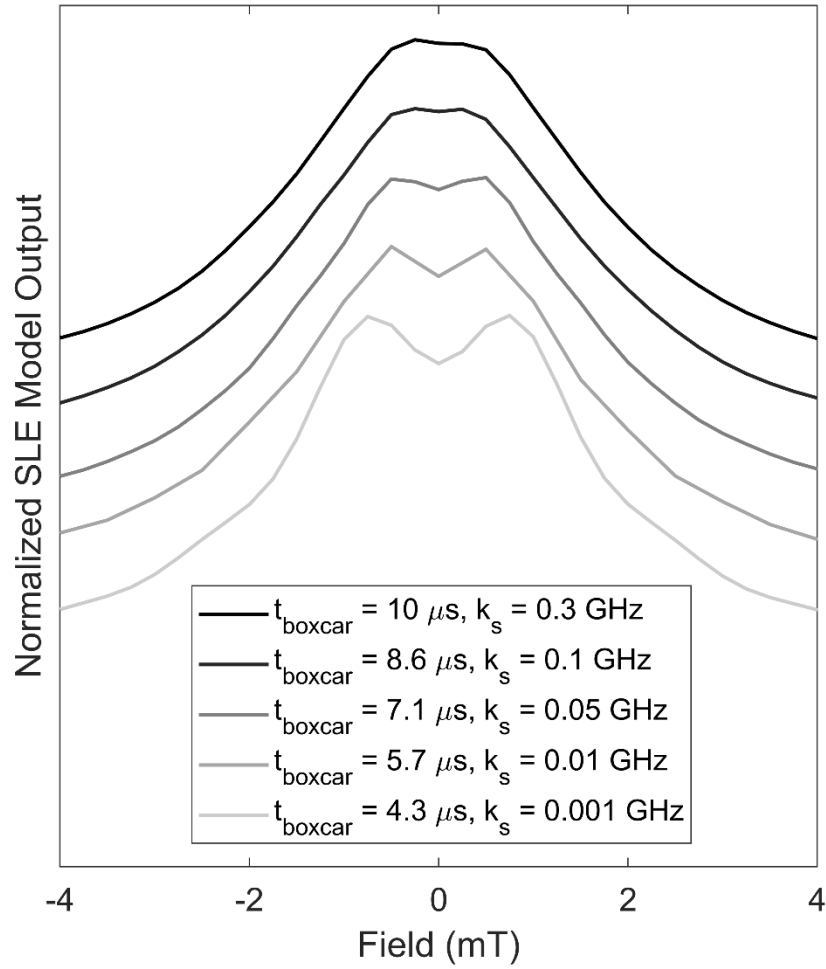defects with varying electron capture time constants.

Fig. 6. Results of SLE simulations with varying t_{boxcar} and k_s. The trend in NZFMR lineshape qualitatively matches those seen in Figures 3-5.

IV.   Discussion

All four NZFMR detection methods are sensitive to the same class of Si/SiO$_2$ interface defect, P$_{b0}$ and P$_{b1}$ centers, and the overall NZFMR lineshape is consistent between the four methods. Varying V_f, F_{cp}, and t_{boxcar} in dc I-V/BAE, CP, and SDTS, respectively, produces

consistent trends in NZFMR broadening and the size of the ultra-low-field feature. SLE modeling of the SDTS NZFMR results qualitatively exhibit the same trends when k_s and t_{boxcar} are varied.

The model for SDTS NZFMR can be conceptually extended to explain the other results in this study if one considers the relationship between the varied parameter, the energy window explored by the measurement, and the density of electrons available for capture. When considering electron capture in an SDTS measurement, the broad energy distribution of P_{b0}/P_{b1} centers creates a spectrum of capture times. By changing t_{boxcar}, the narrow band of energy accessed by the measurement moves up and down in the bandgap. This changes the capture time of the defects observed, with "faster" defects corresponding to a shorter t_{boxcar} and "slower" defects corresponding to a longer t_{boxcar}. It also changes the density of interface electrons available for capture. In the case of dc I-V and BAE, the accessible energy window is directly proportional to V_f[31,32] . Thus, increasing V_f expands the energy window about the middle of the bandgap, effectively uncovering both "faster" and "slower" trapping centers while simultaneously increasing the density of electrons near the interface. Since the capture/recombination process in the DC techniques is continuous, one would expect both the increase in electron density and the involvement of "faster" traps to increase the average rate of the spin-dependent capture. In the case of charge pumping, electron capture is limited by the time spent at V_{high}, which in our case is 40 % of the period of the charge pumping waveform. At the relatively high charge pumping frequencies used here, electron capture time is limited to 400 ns at 1 MHz, 133 ns at 3 MHz, and 80 ns at 5 MHz. In other words, increasing F_{CP} effectively filters out defects with "slower" capture times.

The results of this work have several implications. The agreement in NZFMR lineshape trends between SLE-based modeling and four distinct experimental NZFMR techniques in the same materials system is striking. As stated, NZFMR has already proven useful to semiconductor reliability engineers concerned with the chemical and physical identities of atomic-scale defects at the device level. The above results support the validity of existing SLE-based NZFMR models, and extend the analysis beyond just hyperfine and dipolar coupling constants. Thus far, NZFMR has been used to study defects in Si,[1,5] SiC,[8,22] and a variety of insulators.[2,7,23,25] Such defects can hinder the performance and reliability of devices made from these materials, and they can be proved difficult to study with similar techniques like EDMR[9]. Looking forward, NZFMR could be an important tool for tackling materials physics problems in novel systems such as wide-bandgap semiconductors, 3D integrated circuits, and 2D devices. The widespread tunability of the response across four separate detection techniques highlights the versatility of NZFMR. Our results may allow more concrete conclusions to be drawn about previous device reliability studies that utilized spin-dependent trap-assisted tunneling (SDTAT) NZFMR.[42] Modifying the SLE interpretation to describe hopping rates between neighboring defects in an insulator, rather than the SDR process allows SDTAT NZFMR spectra to be interpreted in a similar way.[4]

Additionally, the NZFMR response has been explored as a potential pathway toward simple and scalable magnetometers.[19] A seminal publication by Cochrane et al. cites the sensitivity of the proposed devices as the chief limiting factor toward further progress. Current NZFMR-based magnetometers utilize SDR in SiC diodes to produce the response and have been aimed at deep-space applications. NZFMR is particularly well-suited for sensing magnetic field on the order of those produced by planetary bodies due to the relatively sharp, ultra-low-field response. To

compete with the state-of-the-art fluxgate magnetometers for these applications, several orders of magnitude of sensitivity improvement are required.[19] The sensitivity of such devices depends on both the size of the response, and its lineshape. Our results demonstrate the effects of biasing conditions on the NZFMR lineshape in great detail and serve as a starting point for future attempts to engineer and model NZFMR responses for magnetometry.

Finally, the behavior of the NZFMR response in Si-based transistors may translate to similar spin-dependent processes which are important to a variety of fields. In recent decades, the field of quantum biology[20,21] has developed, and spin-dependent radical pair mechanisms have been invoked to explain several phenomena. The most prominent example is the mechanism of magnetoreception in a variety of organisms, which is thought to involve the optically-induced, magnetic-field-dependent reaction of radical pairs[43-48]. Much like NZFMR, the rates of such reactions depend on the applied magnetic field strength (whether it be a field applied in the laboratory or Earth's magnetic field), and the interaction of the radicals' unpaired electrons with their local environment. Thus, spin-dependent radical pair interactions are often explained using very similar SLE modeling techniques[43,48]. Similar explanations have been proposed for other biological processes, including the action of Xe-induced general anesthesia. Recently, an isotopic dependence on the efficacy of this anesthesia was found in mice[49]. The effect was later modeled by another group[50].

Given the widespread availability of Si MOSFETs, the relative simplicity of the NZFMR measurement, and the versatile physical framework presented here, we propose that this system has utility as a simulacrum for these more complex phenomena when direct data acquisition is difficult or not feasible.

V.   Conclusion

We demonstrate consistent tunability in the NZFMR response from Si/SiO$_2$ interface defects across a variety of detection techniques in both MOSFETs and capacitors. Simulated results generated from an SLE framework show qualitative agreement with the experimental results, and we connect the parameters varied in the SLE simulations to physical electron capture times at the defect sites. We theorize that the broad energy distribution of P$_{b0}$ defects in the Si bandgap, along with the change in energy range explored by each detection technique, leads to a spread of spin-dependent electron capture rates which affect the NZFMR lineshape. The agreement between modeling and experiment can be extended to a wide range of NZFMR behavior across a variety of detection techniques.

Overall, our results are an important advancement for the more widespread adoption and accessibility of NZFMR-based techniques in studying atomic-scale defect centers in semiconductor devices and materials. The improved theoretical understanding provides the needed framework to draw more meaningful and technically relevant conclusions from experimental results. Our modeling framework accomplishes this within an inexpensive and easy-to-implement measurement setup. We demonstrate aspects of a relatively novel metrology tool- the kind that is required to overcome the incredibly complex materials science and engineering challenges associated with modern semiconductor devices.

Furthermore, our results have a direct impact on other important areas of research unrelated to analytical measurements for defect identification. These include (1) the development of ultra-sensitive magnetometers that exploit the NZFMR response to provide an extremely accurate, sensitive, and self-calibrating measure of magnetic fields and (2) exploiting the NZFMR effect in inexpensive Si-based devices to potentially mimic similar radical pair mechanisms in quantum biology systems.

Conflict of Interest:

The authors have no conflict to disclose.

Data Availability

The data that support the findings of this study are available from the corresponding author upon reasonable request.

References:

[1] C.J. Cochrane, and P.M. Lenahan, "Detection of interfacial Pb centers in Si/SiO_2 metal-oxide-semiconducting field-effect transistors via zero-field spin dependent recombination with observation of precursor pair spin-spin interactions," Appl Phys Lett **103**(5), (2013).

[2] E.B. Frantz, D.J. Michalak, N.J. Harmon, E.M. Henry, S.J. Moxim, M.E. Flatté, S.W. King, J.S. Clarke, and P.M. Lenahan, "Electrically detected magnetic resonance and near-zero field magnetoresistance in $^{28}Si/^{28}SiO_2$," J Appl Phys **130**(6), (2021).

[3] N.J. Harmon, J.P. Ashton, P.M. Lenahan, and M.E. Flatté, "Near-Zero-Field Spin-Dependent Recombination Current and Electrically Detected Magnetic Resonance from the Si/SiO$_2$ interface," (2020), ArXivID: 2008.08121.

[4] E.B. Frantz, N.J. Harmon, S.R. McMillan, S.J. Moxim, M.E. Flatté, and P.M. Lenahan, "Extraction of isotropic electron-nuclear hyperfine coupling constants of paramagnetic point defects from near-zero field magnetoresistance spectra via least squares fitting to models developed from the stochastic quantum Liouville equation," J Appl Phys **128**(12), (2020).

[5] S.J. Moxim, F. V. Sharov, D.R. Hughart, G.S. Haase, C.G. McKay, E.B. Frantz, and P.M. Lenahan, "Near-zero-field magnetoresistance measurements: A simple method to track atomic-scale defects involved in metal-oxide-semiconductor device reliability," Review of Scientific Instruments **93**(11), (2022).

[6] E.B. Frantz, D.J. Michalak, N.J. Harmon, E.M. Henry, M.E. Flatté, S.W. King, J.S. Clarke, and P.M. Lenahan, "Effects of ^{29}Si and ^{1}H on the near-zero field magnetoresistance response of Si/SiO$_2$ interface states: Implications for oxide tunneling currents," Appl Phys Lett **119**(18), (2021).

[7] E.B. Frantz, N.J. Harmon, D.J. Michalak, E.M. Henry, M.E. Flatté, S.W. King, J.S. Clarke, and P.M. Lenahan, "Extraction of dipolar coupling constants from low-frequency electrically detected magnetic resonance and near-zero field magnetoresistance spectra via least squares fitting to models developed from the stochastic quantum Liouville equation," J Appl Phys **130**(23), (2021).

[8] M.A. Anders, P.M. Lenahan, N.J. Harmon, and M.E. Flatté, "A technique to measure spin-dependent trapping events at the metal-oxide-semiconductor field-effect transistor interface: Near zero field spin-dependent charge pumping," J Appl Phys **128**(24), (2020).

[9] J.P. Ashton, S.J. Moxim, P.M. Lenahan, C.G. McKay, R.J. Waskiewicz, K.J. Myers, M.E. Flatte, N.J. Harmon, and C.D. Young, "A new analytical tool for the study of radiation effects in 3-D integrated circuits: Near-zero field magnetoresistance spectroscopy," IEEE Trans Nucl Sci **66**(1), 428–436 (2019).

[10] N.J. Harmon, and M.E. Flatté, "Semiclassical theory of magnetoresistance in positionally disordered organic semiconductors," Phys Rev B Condens Matter Mater Phys **85**(7), (2012).

[11] N.J. Harmon, and M.E. Flatté, "Organic magnetoresistance from deep traps," J Appl Phys **116**(4), (2014).

[12] N.J. Harmon, and M.E. Flatté, "Spin-flip induced magnetoresistance in positionally disordered organic solids," Phys Rev Lett **108**(18), (2012).

[13] A.J. Schellekens, W. Wagemans, S.P. Kersten, P.A. Bobbert, and B. Koopmans, "Microscopic modeling of magnetic-field effects on charge transport in organic semiconductors," Phys Rev B Condens Matter Mater Phys **84**(7), (2011).

[14] W. Wagemans, A.J. Schellekens, M. Kemper, F.L. Bloom, P.A. Bobbert, and B. Koopmans, "Spin-spin interactions in organic magnetoresistance probed by angle-dependent measurements," Phys Rev Lett **106**(19), (2011).

[15] P.A. Bobbert, T.D. Nguyen, F.W.A. Van Oost, B. Koopmans, and M. Wohlgenannt, "Bipolaron mechanism for organic magnetoresistance," Phys Rev Lett **99**(21), (2007).

[16] V.N. Prigodin, J.D. Bergeson, D.M. Lincoln, and A.J. Epstein, "Anomalous room temperature magnetoresistance in organic semiconductors," Synth Met **156**(9–10), 757–761 (2006).

[17] P. Desai, P. Shakya, T. Kreouzis, W.P. Gillin, N.A. Morley, and M.R.J. Gibbs, "Magnetoresistance and efficiency measurements of Alq3 -based OLEDs," Phys Rev B Condensed Matter Phys **75**(9), (2007).

[18] N.J. Harmon, J.P. Ashton, P.M. Lenahan, and M.E. Flatté, "Spin-dependent capture mechanism for magnetic field effects on interface recombination current in semiconductor devices," App Phys Lett **123**(25), (2023).

[19] C.J. Cochrane, J. Blacksberg, M.A. Anders, and P.M. Lenahan, "Vectorized magnetometer for space applications using electrical readout of atomic scale defects in silicon carbide," Sci Rep **6**, (2016).

[20] N. Lambert, Y.N. Chen, Y.C. Cheng, C.M. Li, G.Y. Chen, and F. Nori, "Quantum biology," Nat Phys **9**(1), 10–18 (2013).

[21] Y. Kim, F. Bertagna, E.M. D'souza, D.J. Heyes, L.O. Johannissen, E.T. Nery, A. Pantelias, A.S.P. Jimenez, L. Slocombe, M.G. Spencer, J. Al-Khalili, G.S. Engel, S. Hay, S.M. Hingley-Wilson, K. Jeevaratnam, A.R. Jones, D.R. Kattnig, R. Lewis, M. Sacchi, N.S. Scrutton, S.R.P. Silva, and J. McFadden, "Quantum biology: An update and perspective," Quantum Reports **3**(1), (2021).

[22] C.J. Cochrane, and P.M. Lenahan, "Zero-field detection of spin dependent recombination with direct observation of electron nuclear hyperfine interactions in the absence of an oscillating electromagnetic field," J Appl Phys **112**(12), (2012).

[23] S.J. Moxim, J.P. Ashton, P.M. Lenahan, M.E. Flatte, N.J. Harmon, and S.W. King, "Observation of Radiation-Induced Leakage Current Defects in MOS Oxides with Multifrequency Electrically Detected Magnetic Resonance and Near-Zero-Field Magnetoresistance," IEEE Trans Nucl Sci **67**(1), 228–233 (2020).

[24] M.A. Anders, P.M. Lenahan, C.J. Cochrane, and J. Van Tol, "Physical nature of electrically detected magnetic resonance through spin dependent trap assisted tunneling in insulators," J Appl Phys **124**(21), (2018).

[25] M.J. Mutch, P.M. Lenahan, and S.W. King, "Spin transport, magnetoresistance, and electrically detected magnetic resonance in amorphous hydrogenated silicon nitride," Appl Phys Lett **109**(6), (2016).

[26] D.J. Lepine, "Spin-Dependent Recombination on Silicon Surface," Phys Rev B **6**(2), (1972).

[27] F.C. Rong, W.R. Buchwald, E.H. Poindexter, W.L. Warren, and D.J. Keeble, "Spin-dependent Shockley-Read recombination of electrons and holes in indirect band-gap semiconductor p-n junction diodes," Solid State Electronics **34**(8), (1991).

[28] D. Kaplan, I. Solomon, and N.F. Mott, "Explanation of the Large Spin-Dependent Recombination Effect in Semiconductors," J Phys (Paris) Lett **39**(4), (1978).

[29] M. Hori, and Y. Ono, "Charge Pumping under Spin Resonance in Si (100) Metal-Oxide-Semiconductor Transistors," Phys Rev Appl **11**(6), (2019).

[30] W. Shockley, and W.T. Read, "Statistics of the Recombinations of Holes and Electrons," Physical Review **87**(5), (1952).

[31] J. Fitzgerald, and A.S. Grove, "Surface Recombination in Semiconductors," Surf Sci **9**, 347–369 (1968).

[32] J.P. Ashton, S.J. Moxim, A.D. Purcell, P.M. Lenahan, and J.T. Ryan, "A quantitative model for the bipolar amplification effect: A new method to determine semiconductor/oxide interface state densities," J Appl Phys **130**(13), (2021).

[33] J.S. Brugler, and P.G.A. Jespers, "Charge pumping in MOS devices," IEEE Trans Electron Devices **16**(3), 297–302 (1969).

[34] M.C. Chen, and D. V Lang, "Observation of Spin-Dependent Thermal Emission from Deep Levels in Semiconductors," Phys Rev Lett **51**(5), (1983).

[35] K.J. Myers, P.M. Lenahan, J.P. Ashton, and J.T. Ryan, "A new approach to electrically detected magnetic resonance: Spin-dependent transient spectroscopy," J Appl Phys **132**(11), 115301 (2022).

[36] Y. NIshi, K. Tanaka, and A. Ohwada, "Study of silicon-silicon dioxide structure by electron spin resonance I," Jpn J Appl Phys **10**(52), (1971).

[37] Y.Y. Kim, and P.M. Lenahan, "Electron-spin-resonance study of radiation-induced paramagnetic defects in oxides grown on (100) silicon substrates," J Appl Phys **64**(7), 3551–3557 (1988).

[38] P.M. Lenahan, "What can electron paramagnetic resonance tell us about the Si/SiO$_2$ system?," Journal of Vacuum Science & Technology B: Microelectronics and Nanometer Structures **16**(4), 2134 (1998).

[39] G.J. Gerardi, E.H. Poindexter, P.J. Caplan, and N.M. Johnson, "Interface traps and P$_b$ centers in oxidized (100) silicon wafers," Appl Phys Lett **49**(6), 348–350 (1986).

[40] S.J. Moxim, F. V. Sharov, D.R. Hughart, G.S. Haase, C.G. McKay, and P.M. Lenahan, "Atomic-scale defects generated in the early/intermediate stages of dielectric breakdown in Si/SiO$_2$ transistors," Appl Phys Lett **120**(6), (2022).

[41] J.P. Campbell, P.M. Lenahan, C.J. Cochrane, A.T. Krishnan, and S. Krishnan, "Atomic-scale defects involved in the negative-bias temperature instability," IEEE Transactions on Device and Materials Reliability **7**(4), 540–557 (2007).

[42] F. V. Sharov, S.J. Moxim, G.S. Haase, D.R. Hughart, C.G. McKay, and P.M. Lenahan, "Probing the Atomic-Scale Mechanisms of Time-Dependent Dielectric Breakdown in Si/SiO$_2$ MOSFETs (June 2022)," IEEE Transactions on Device and Materials Reliability **22**(3), 322–331 (2022).

[43] S. Worster, D.R. Kattnig, and P.J. Hore, "Spin relaxation of radicals in cryptochrome and its role in avian magnetoreception," Journal of Chemical Physics **145**(3), (2016).

[44] T. Ritz, S. Adem, and K. Schulten, "A model for photoreceptor-based magnetoreception in birds," Biophys J **78**(2), 707–718 (2000).

[45] M. Tiersch, and H.J. Briegel, "Decoherence in the chemical compass: The role of decoherence for avian magnetoreception," Philosophical Transactions of the Royal Society A: Mathematical, Physical and Engineering Sciences **370**(1975), 4517–4540 (2012).

[46] S.Y. Wong, Y. Wei, H. Mouritsen, I.A. Solov'Yov, and P.J. Hore, "Cryptochrome magnetoreception: Four tryptophans could be better than three," J R Soc Interface **18**(184), (2021).

[47] I.A. Solov'yov, and K. Schulten, "Magnetoreception through cryptochrome may involve superoxide," Biophys J **96**(12), 4804–4813 (2009).

[48] T. Ritz, P. Thalau, J.B. Phillips, R. Wiltschko, and W. Wiltschko, "Resonance effects indicate a radical-pair mechanism for avian magnetic compass," Nature **429**(6988), 174–177 (2004).

[49] N. Li, D. Lu, L. Yang, H. Tao, Y. Xu, C. Wang, L. Fu, H. Liu, Y. Chummum, and S. Zhang, "Nuclear spin attenuates the anesthetic potency of xenon isotopes in mice: Implications for the mechanisms of anesthesia and consciousness," Anesthesiology **129**(2), 271–277 (2018).

[50] J. Smith, H. Zadeh Haghighi, D. Salahub, and C. Simon, "Radical pairs may play a role in xenon-induced general anesthesia," Sci Rep **11**(1), (2021).